water

MDPI

Article

Change Analysis of Karst Landforms, Hydrogeological Conditions and Effects of Tunnel Excavation on Groundwater Environment in Three Topography Grades in China

Yige Tang [1], Qiang Zhang [1,*], Jihong Qi [1], Mo Xu [1], Xiao Li [1], Chenhao Qu [1], Lei Yi [1] and Dong Wang [2]

[1] State Key Laboratory of Geohazard Prevention and Geoenvironment Protection, Chengdu University of Technology, Chengdu 610059, China
[2] China Railway Eryuan Engineering Group Co., Ltd., Chengdu 610031, China
* Correspondence: zhangq@cdut.edu.cn

Abstract: One-third of the Earth in China is formed by Karst topography, which exposes different Karst landforms in three topography grades from southeast to northwest, corresponding to below several hundred meters for the first grade, one to two thousand meters for the second grade, and more than 4000 m for the in Qinghai-Tibet Plateau. Through the hydrochemical and D-^{18}O stable isotopes of 64 water samples collected along two railway lines and the topography fractal characteristics of three typical Karst areas in different topography grades, the changes in Karst development degree, changes in groundwater activities, and the influence of tunnel excavation effects on groundwater environment were analyzed. The results indicated that: (1) the Karst development degree and the influence of Karst tunnel excavation on the groundwater environment are somehow similar in the first and second grades, while there are significant differences between the slopes area from second to third grade and the third grade area. (2) In detail, the relatively weaker Karst development degree and flow seeping in the second grade relatively weaken the influences of tunnel excavation, including the distribution pattern of water resources, the groundwater flow field, and water circulation, while the tunnel elevation has little room to rise. (3) There are many large faults in the north-southward direction in the third topography grade, and the transportation lines in the eastern-western direction will inevitably encounter them. In the intersection area, the tunnel excavation has great effects on the groundwater environment. (4) The lighter hydrogen and oxygen isotopes are enriched in Karst water from the first grade to the third grade, indicating that the recharge source of Karst water presents obvious elevation effect.

Keywords: Karst landforms; topography grades; tunnel excavation; Qinghai-Tibet Plateau; groundwater environment

Citation: Tang, Y.; Zhang, Q.; Qi, J.; Xu, M.; Li, X.; Qu, C.; Yi, L.; Wang, D. Change Analysis of Karst Landforms, Hydrogeological Conditions and Effects of Tunnel Excavation on Groundwater Environment in Three Topography Grades in China. *Water* **2023**, *15*, 207. https://doi.org/10.3390/w15010207

Academic Editor: David Labat

Received: 24 November 2022
Revised: 28 December 2022
Accepted: 28 December 2022
Published: 3 January 2023

1. Introduction

Karst covers approximately one-third of the Earth in China. As the altitude rises, different Karst landforms are exposed [1]. Topography altitudes are divided into three grades from southeast to northwest in China. The areas of the first grade have an altitude of about several hundred meters and are mostly distributed in the southeast area such as Guangxi Province and Yun-Gui Plateau situates. The areas of the second grade have an altitude of one to two thousand meters. The highest-level area is located in Qinghai-Tibet Plateau situates, which are more than 4000 m high. The distribution of the three grades is shown in Figure 1 [2,3]. In southern China, there are four typical types of Karst landform compositions, including peak-cluster with depression (the funnel), peak-forest with depression, isolate peak (residual hillock) with Karst plain, and Karst hill with depression. The first three types show landform diversity from Guangxi Province to Yun-Gui Plateau [4,5]. Shallow dish with Hillock becomes the main Karst landform composition in the central area of Yun-Gui Plateau [1]. There are two different viewpoints about Karst

landforms in Qinghai-Tibet. Some researchers consider the palaeo Karst of Qinghai-Tibet as the covered Karst. They believe most of the landforms have already been destroyed with topographical uplift, and current Karst features include some stone pinnacles and rock walls [6–9]. While others consider that the recognizable Karst features in Qinghai-Tibet Plateau are small caves and corrosion fissures formed by physical weathering under the condition of Quaternary periglacial climate [10,11]. Both opinions acknowledge that there are few typical Karst landforms in this area.

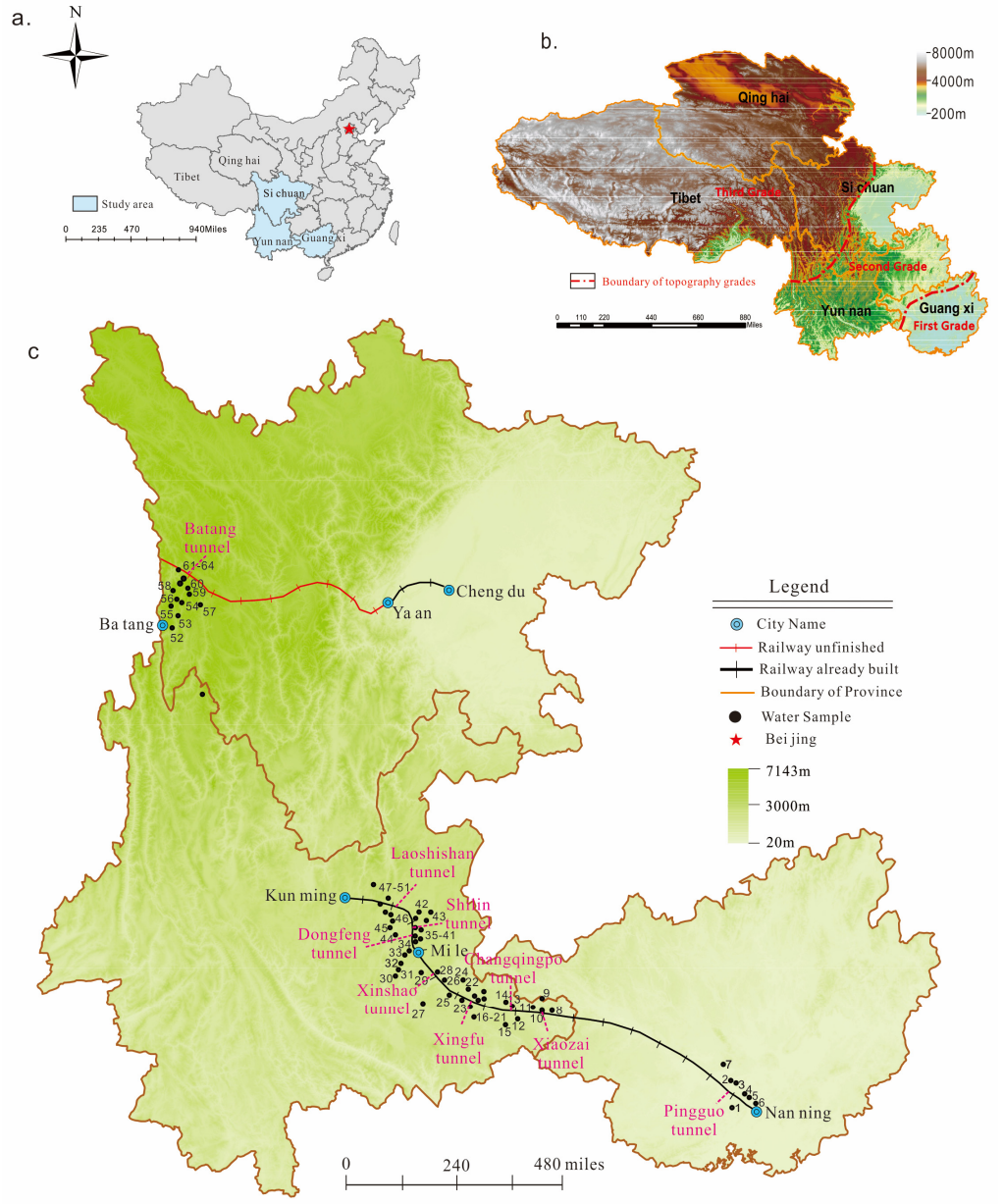

Figure 1. (**a**) Distribution map of provinces in China and Study area. (**b**) Three altitude grades of topography in the study area ranging from 200 m to over 5000 m. (**c**) Water sample location and tunnel distribution.

The huge altitude difference between these three grades becomes an insurmountable barrier for transportation [12]. As a result, tunnel excavation has become a common need for efficient transportation in the forms of expressways and railways in the Karst plateau and mountain areas [13,14], and consequently, there are a large number of tunnels in southwest China [12]. The depths of tunnels are generally tens of meters to hundreds of meters, and some in the world even exceed 1000 m [15]. The depth of the diversion tunnel of Jinping

Hydropower Station in China is 2525 m, which has been designed and is to be constructed [16]. In addition, the railway from Sichuan to Lasa situates on the Qinghai-Tibet Plateau, and the design depth of some Karst tunnels is greater than 2000 m. By the end of 2018, there are 3896 tunnels with a total length of 4300 km in carbonate area [12]. The most significant hydrogeological impact of the tunnel excavation in an aquifer is the drainage effect [17]. If the tunnel is located below the regional groundwater level, springs or underground rivers may be drained, and the groundwater level will drop significantly, which can lead to hydrogeological and environmental impacts on groundwater-dependent ecosystems [18].

Karst environments are characterized by unique landforms related to dissolution and dominant subsurface drainage, which can affect the groundwater flow characteristics [19]. In another word, the most significant hydrogeological impacts, such as barrier and drain effects in an aquifer, are influenced by the Karst development degree and the characteristics of groundwater flow [19]. The barrier effect causes the water table to rise in the upper reaches and the water table to drop in the down reaches [20,21]. The drain effect can extract groundwater, reduce the groundwater table, and cause some environmental and geotechnical consequences [22–24]. In this study, we investigated three typical hydrogeology systems along two railways, as shown in Figure 1b,c. The three hydrogeology systems cross the Karst area and are distributed in three topography grades. The geochemistry, isotope characteristics, and geomorphology analysis methods were used to analyze the relationship between Karst landforms and the characteristics of ground flow, including the characteristics of groundwater, hydraulic connection, and hydrodynamic conditions. Then we discussed the changes in Karst development degree, the activities of groundwater, and the effects of tunnel excavation on the groundwater environment in different hydrogeology grades. The results can suggest a better tunnel layout to avoid or reduce the impact of tunnel excavation.

2. Methods

2.1. Hydrochemistry and Isotope Analyses

In August 2011 and August 2018, a series of samples, consisting of some springs, surface water, underground river water, and two warm springs, were collected in the areas where railway lines pass. The locations of samples are shown in Figure 1b. Three typical tunnels, i.e., Pingguo Tunnel, Dongfeng Tunnel, and Batang tunnel, are located in the three topography grades with different Karst landforms. The samples were collected in the strata, including Silurian, Devonian, Carboniferous, Permian System, and Triassic.

All indoor analyses were rapidly performed in the aqueous chemistry facility operated by the Chengdu University of Technology. Anions and cations were analyzed using DIONEX (ICS-1100) and ICP-OES (ICAP6300), respectively. The stable isotopic composition of hydrogen and oxygen was determined by the Isotopic Laboratory of the China Geological Survey. The standard deviation of the isotopic analyses (MAT 253 stable isotope ratio mass spectrometer) is $\pm 0.2‰$ for $\delta^{18}O$ and $\pm 2‰$ for δD.

2.2. Fractal Characteristics of the Karst Landforms

The morphological parameter statistics and fractal characteristics were used to study the Karst development degrees, including morphological parameter statistics of Karst peak, as well as the fractal dimension of Karst depression and contour. The Karst development progress can be divided into three periods, i.e., juvenile stage, maturity stage, and old stage, corresponding to different Karst morphological features, namely, peak–cluster, peak–forest, and isolate peak, as shown in Figure 2 [25,26]. The shape of the curve of N(δ) versus δ can be used to study the Karst development stage. Based on the different height standards (δ), the number of peaks (N(δ)) exceeding the height standard can be counted, and the curve of N(δ) versus δ can be constructed.

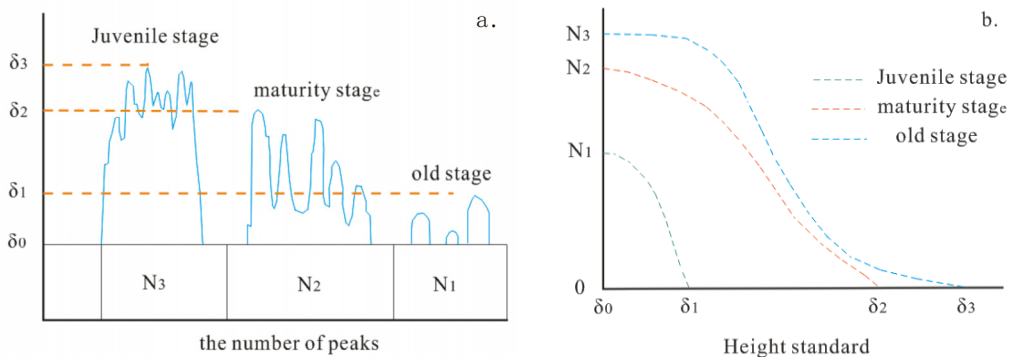

Figure 2. (**a**) Relationship between the number of Karst peaks and Karst development stages. (**b**) Relationship between the height standards and Karst development stages.

The number of Karst peaks (N(δ)) based on the height standard (δ) for different Karst development stages; N_1, N_2, and N_3 represent the number of Karst peaks for the juvenile stage, maturity stage, and old stage, respectively; δ_1, δ_2, and δ_3 represent the height standards of Karst peaks for Juvenile stage, maturity stage, and old stage, respectively.

Relationship curves between the number of Karst peaks of the height standard (δ) for different Karst development stages are represented.

The morphology of Karst depression and contour is divided into three grades (Figures 3 and 4) [25]. The smoother the depression boundary, the stronger the Karst development. The smoother the contour, the weaker the Karst development. Based on the morphology datum, the perimeter and area of Karst depressions can be measured, and Equation (1) can be used to obtain the fractal dimension of Karst depressions.

$$D = 2\frac{LogL(\delta)}{LogA(\delta)} \quad (1)$$

where D is the fractal dimension, δ is the length standard, L(δ) is the perimeter of the depression based on the different length standards, and A(δ) is the area of depression based on the square area δ^2. According to the range of D values from 1 to 2, the Karst development can be divided into three stages. The strongest stage has the smallest value of D, and the weakest stage has the largest value of D.

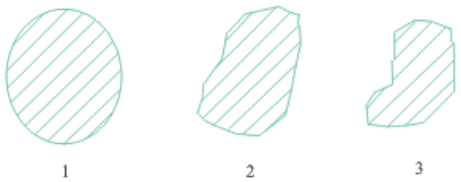

Figure 3. The morphology of Karst depressions for different Karst stages 1, 2, and 3 represent three Karst development stages from strong to weak degree.

Figure 4. The morphology of contour for different Karst stages 1, 2, and 3 represent three Karst development stages from strong to weak degree.

Based on the different length standards (δ), the numbers of segmentations (N(δ)) can be determined, and the fractal dimension is defined as the gradient of line relationship between lnN(δ) and δ. The higher the gradient, the more complex the topography, and the stronger the Karst development.

3. Description of the Study Site

The study was carried out along the area of three typical railway tunnels within two railway lines (Figure 1b,c). Line ①, Yun-Gui railway, is located from the lowest to the second topography grade, and Line ②, Western Sichuan traffic corridor, is located in the slope zone between the second and highest topography grades. The geological characteristics of these three railway tunnels are summarized as follows:

Pingguo Tunnel in railway line ① passes a zone with a typical landscape of peak-cluster and depression (Figure 5a), and the elevation of this area ranges from ~100 to 800 m. The rivers flow around the Karst mountains, following the direction of strata extension. The Devonian and Carboniferous strata are located in the eastern area, and the Permian stratum is located in the western area and is cut by the Youjiang River. The total thickness of Devonian and Carboniferous strata is about 500~1600 m. Limestone dominates and is interbedded with dolomite, which is the main lithology in this area. Some springs with a large volume of water appear near the banks of the river, and there are two Karst tunnels with several ponors lying above. Faults are relatively limited in the region, and their extension direction is consistent with the strata, thus making them a potential groundwater runoff channel.

Dongfeng Tunnel in railway line ① passes the zone with shallow depressions and dwarf hills (Figure 5b), and the elevation of this area is about 1500~2600 m. This area is mainly covered by the early Paleozoic Cambrian and Devonian strata, whose lithology is dolomite and impure limestone. Groundwater is buried more deeply in the middle area. Some springs with a volume of 1.2 to 10 L/s appear where rivers cut the rocks at the boundary of this system. The groundwater in this area discharges more dispersedly. The northeast striking regional fault forms a lower terrain, and the lithological variations become the confining boundary, and most of the groundwater discharges nearby.

The tunnel lithology information is shown in Figure 6. Batang Tunnel crosses the plateau canyon landscape (Figure 5c), and the altitude difference can reach 2500 m. In this area, some big glacially eroded depressions and sharp peaks appear, and some long and wide dissolution fissures are also found in rocks. However, Karst caves and holes are rare. Paleozoic strata of crystalline limestone and marble are the main strata here. Two big fracture systems extend from north to south in this area, which has strong water-bearing characteristics. A large regional fault forms multiple parallel branches in the area, as well as most the groundwater transport along the fault. When the rivers and valleys cut the fracture system, some springs with big water flow are found. About 70% of the Karst phenomenon, including springs with a volume of 5 to 500 L/s and small Karst caves, are located at the fault or close to it.

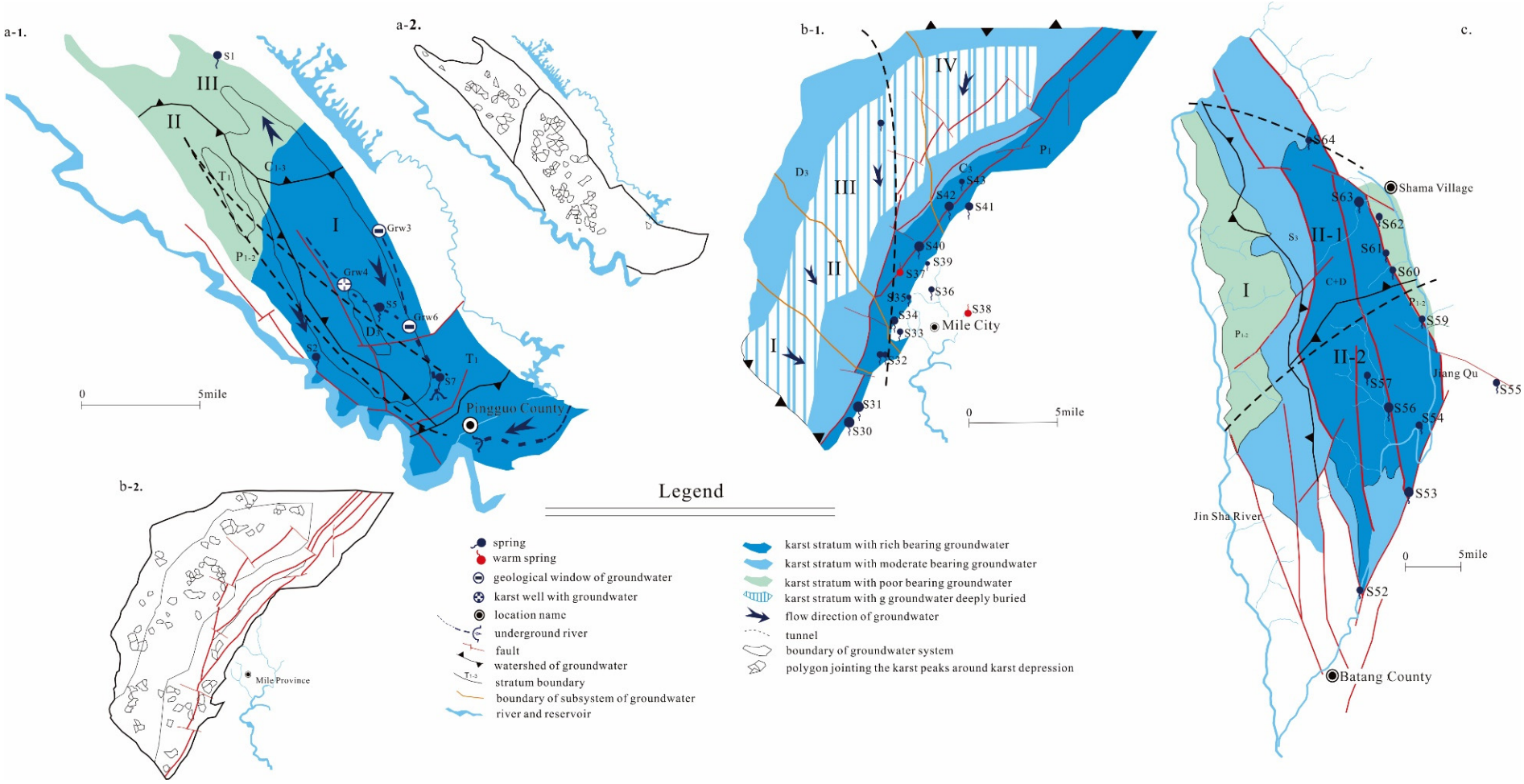

Figure 5. The typical hydrogeological system for three topography grades and tunnel layout. (**a-1**). Layout of the Pingguo tunnel and the hydrogeology systems located in the first topography area; (**a-2**). The polygon distribution jointing the Karst peaks around Karst depressions. (**b-1**). Layout of the Dongfeng tunnel and the hydrogeology systems in the second topography area; (**c**). Layout of the Batang tunnel and the hydrogeologic system in the third topography area. (**a-2**,**b-2**) are used to obtain the fractal dimension representing the Karst development degree.

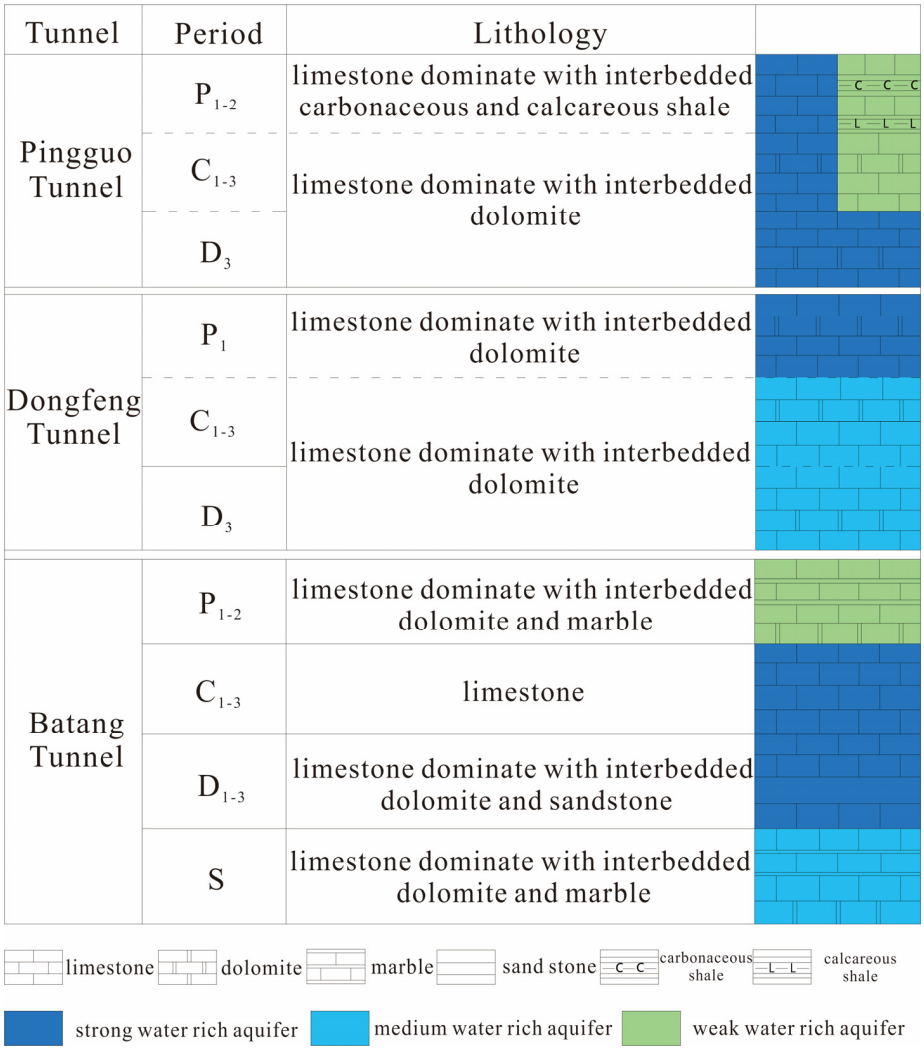

Figure 6. Lithology and water-bearing characteristics of study areas traversed by three typical railroad tunnels.

4. Results

4.1. Chemical and Isotope Characteristics of Groundwater

The saturation index of calcium carbonate (SI-$CaCO_3$) of 64 samples is shown in Figure 7. The value of SI-$CaCO_3$ ranges from −2.448 to 0.7429. The SI-$CaCO_3$ of the surface river and underground river are lowest in zone ⑤. Both surface and subsurface rivers are unsaturated, and SI-$CaCO_3$ of the underground river is higher than that of the surface river. SI-$CaCO_3$ of groundwater samples decreases from southeast to northwest and can be divided into four zones. The SI-$CaCO_3$ of zone ① is greater than zero, indicating that the Karst groundwater in the south area can be saturated. The SI-$CaCO_3$ of zones ②, ③, and ④ are less than zero, indicating the Karst groundwater samples in this area, especially the groundwater samples from the northwest area, are unsaturated. The lowest SI of this area is about −0.75, which is higher than the SI-$CaCO_3$ of rivers.

The relationship between $\delta^{18}O$ and δD is plotted in Figure 8, which also shows the global meteoric water line with $\delta D = 8\delta^{18}O + 10$ [27], the Southwestern China meteoric line with $\delta D = 1.96\delta^{18}O + 9.53$ [28], and the meteoric water line in the middle-lower region of the Yarlung Zangbu River with $\delta D = 7.54\delta^{18}O + 15.92$ [29]. The trend line of all samples is also plotted in this figure, which is $\delta D = 7.704\delta^{18}O + 3.95$, and the value of R^2 is 0.96.

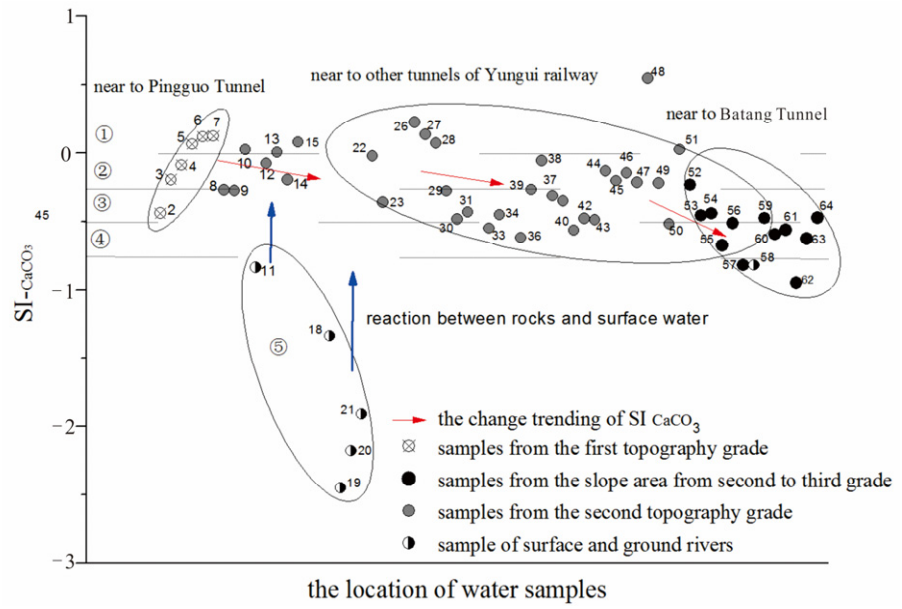

Figure 7. SI-$_{CaCO3}$ of calcium carbonate in samples. ① SI ranges from 0 to 0.25; ② SI ranges from −0.25 to 0; ③ SI ranges from −0.5 to−0.25; ④ SI ranges from −0.5 to −0.75.

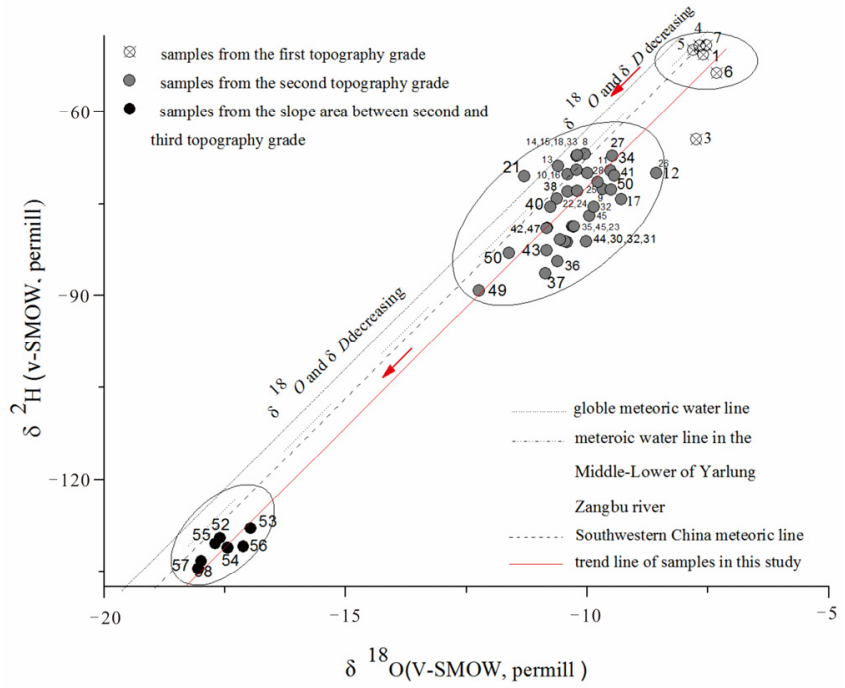

Figure 8. Relationship between δ^{18}O (V−SMOW, permill) and δ^{2}H (V−SMOW, permill).

Most of the samples are located near the globe meteoric water line, and even two warm springs of No. 37 and No. 38, δ^{18}O values do not show positive shifts, and the δ^{18}O well responds to elevation change. The elevation effect of $\delta^{18}O$ (Equation (2)) [30] can infer the supply altitude of groundwater. The distribution of δ^{18}O vs. δD is clearly in three zones.

$$\frac{H_* - H_0}{100 \times \left(\delta^{18}O_* - \delta^{18}O_0\right)} = -0.27‰ \quad (2)$$

where H_* and H_0 represent the altitude of the analysis sample and standard sample, respectively; $\delta^{18}O_*$ and $\delta^{18}O_0$ come from the analysis sample and standard sample, respectively.

The elevation difference between the supply area and the appearing area is shown in Figure 9. From the figure, the elevation difference increases from the southeast to the northwest. The southeast area locates in the lowest topography grade, and the elevation ranges from 194 m to 419 m, with a difference of smaller than 500 m. The northwest area locates in the highest topography grade, and the largest elevation difference can reach 2213 m. The middle area locates in the second topography grade with an elevation gap of up to 704 m, and about half of the springs' elevations are more than 500 m.

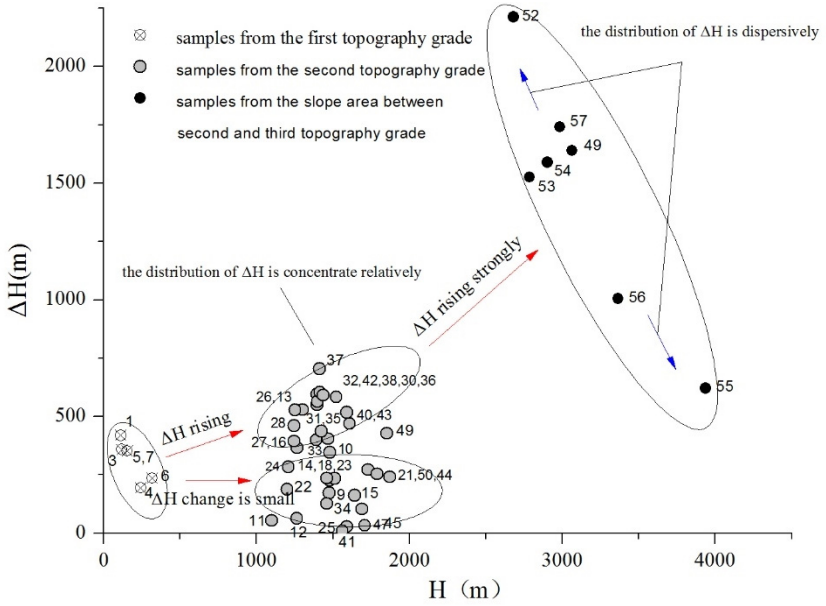

Figure 9. Elevation difference between supply area and appearing area of water samples.

ΔH is the difference between supply and appearing elevations of groundwater, and H is the appearing elevation of groundwater.

4.2. The Equilibrium of Ca^{2+}

(1) Pingguo System

Pingguo Tunnel is located in the northwest area of Pingguo Province county, as shown in Figure 5(a-1). This area lies in the lowest topography grade area of China. The insoluble stratum and rivers are considered boundaries of the hydrogeological system through which the tunnel passes. The area of this system is about 141 km^2. According to the water-bearing characteristics of groundwater, this area can be divided into two regions, i.e., the southeastern region with strong groundwater bearing characteristics and the northwestern region with weak groundwater bearing characteristics. The typical Karst landscapes in this area include peak forests, isolated peaks, and depressions. Two underground rivers are lying in the south area, with several geological windows connected with them. The water samples in this area include some springs and groundwater from the geological windows, as shown in Figure 5(a-1).

This area is divided into three subsystems of groundwater, as shown in Figure 5(a-1). The saturation index of calcium carbonate has the same trend as that of the concentration of Ca^{2+}. In the sub-hydrogeology system, No. 5 and No. 7 are spring water, and No. 3, No. 4, and No. 6 are underground water collected through the geological windows. The concentration of Ca^{2+} in the samples is in the order of No. 3 < No. 4 < No. 5 < No. 6 < No. 7, while the SI-$CaCO_3$ is in the order of No. 2 < No. 3 < No. 4 < No. 7 < No. 6. These trends indicate that the flow direction is from the northwestern region to the southeastern region, as shown in Figure 5(a-1). It supports the subsystems division of geology. The layout of the two tunnels is shown in Figure 10a. The north layout crosses the subsystem, while the south layout does not cross the subsystem.

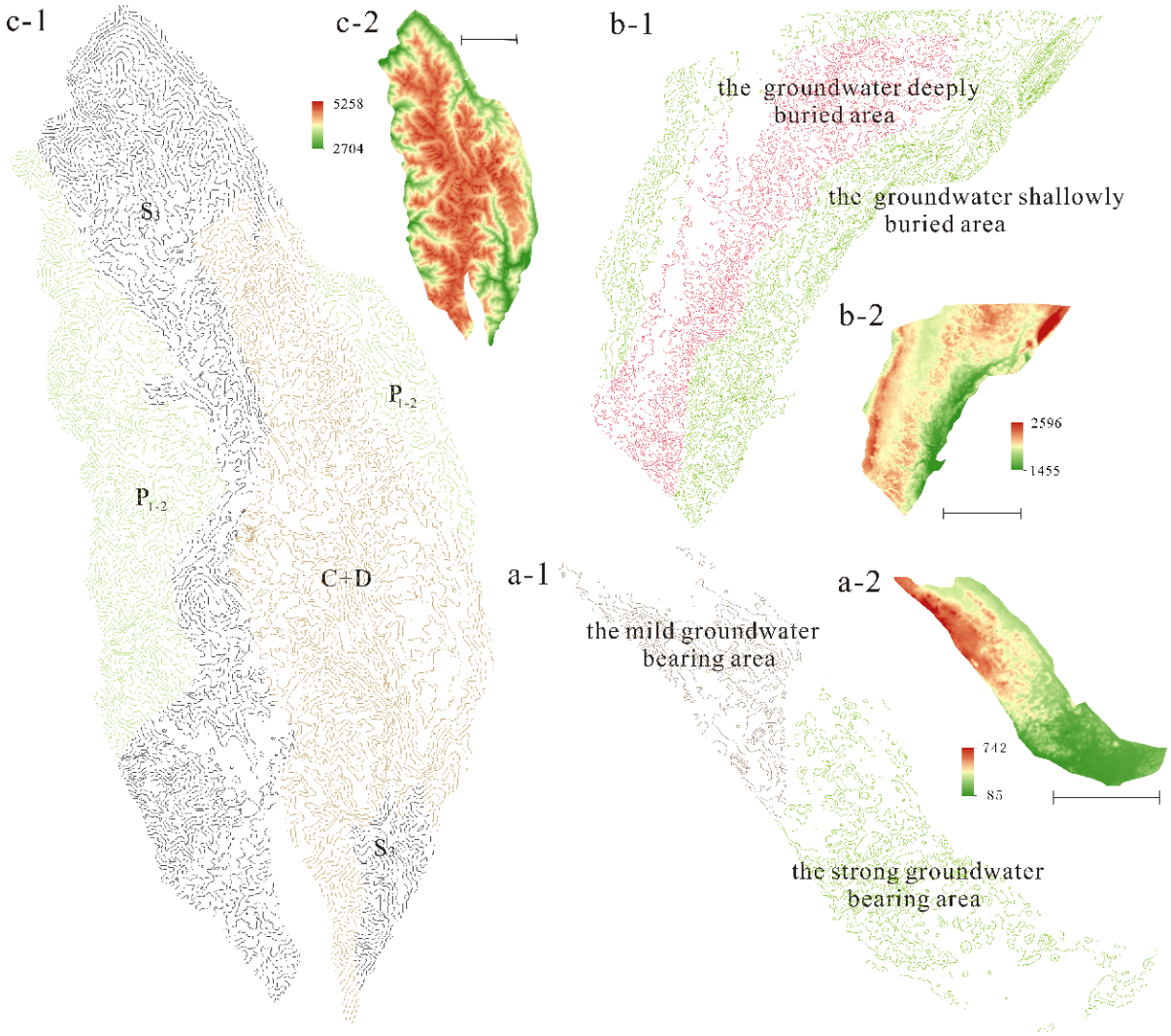

Figure 10. The altitude distribution and the contours in three typical study areas (the data come from the SRTMDEM 90M given by Geospatial Data Cloud, and these data are used to obtain the fractal Dimensions). (**a-1**,**a-2**) are for Pingguo System, which is divided into the strong groundwater bearing area and mild groundwater bearing area. (**b-1**,**b-2**) are for Dongfeng System, which is divided into deeply buried groundwater and shallowly buried groundwater. (**c-1**,**c-2**) are for Batang system, which is divided into a strong water-bearing stratum (C + D), a moderate water-bearing stratum (S), and the weak water-bearing stratum (P_{1-2}).

(2) Dongfeng System

Dongfeng Tunnel is located in the west area of Mile County in Yunnan Province, as shown in Figure 5(b-1). This area lies in the second topography grade area of China. The insoluble rock and topography watershed are considered the boundaries of the hydrogeological system through which the tunnel passes. The area of this system is about 739.5 km^2. The groundwater-bearing characteristics are used to divide this area into three parts, and the strata of Carboniferous and Devonian are divided into two zones. The deeply buried groundwater is in the middle zone of this water-bearing stratum, while shallowly buried groundwater is in the surrounding zone. The stratum of Permian has strong groundwater-bearing characteristics and lies in the east area near the strata of Carboniferous and Devonian. The water samples in this area include 14 springs including two warm springs, and most of them appear in the stratum of Permian, and the boundary between the Permian stratum and Quaternary is shown in Figure 5(b-1).

In this hydrogeological system, the saturation index of Calcium carbonate is all below zero, ranging from −0.6168 to −0.0558. In every subsystem, the SI and the concentration of Ca^{2+} do not have obvious differences, and both are lower than those of the hydrogeology system of the Pingguo System.

(3) Batang System

Batang Tunnel is located in the western area of Batang County, close to the boundary between Sichuan Province and Tibet, as shown in Figure 5c. This area lies in the slope zone from the second to first topography grade area. The insoluble rock and rivers are considered the boundaries of the groundwater system, through which the tunnel passes. The area of this system is about 1521.2 km^2. The groundwater-bearing characteristics can be divided into three grades. The strata of Carboniferous and Devonian have the strongest groundwater-bearing characteristics, followed by the Silurian stratum, and the stratum of Permian has the weakest characteristics. Thirteen water samples were collected in this area, including springs and surface water. Most of the samples were from the strata of Carboniferous and Devonian along the faults, and some samples were collected from the boundary area between the stratum of Permian and the insoluble rock, as shown in Figure 5c.

In this hydrogeological system, the saturation index of calcium carbonate is below zero, ranging from −1.3161 to −0.2733. This hydrogeological system has a significantly lower saturation index than the hydrogeology system of the Dongfeng System. The SI-$CaCO_3$ in subsystem II-2 has the trend of No. 57 < No. 56 < No. 53 < No. 52. In contrast, in subsystem II-1, the SI-$CaCO_3$ has the trend of No. 62 < No. 61 < No. 60 < No. 59. In these subsystems, the concentration of calcite trended opposite to SI-$CaCO_3$.

4.3. Fractal Characteristics of Typical Karst Areas

In this study, the topography data of SRTMDE.M 90M were used to count the area and circumference of the polygon connecting the Karst peaks and saddle zones around Karst depressions. There are 99 Karst depressions in the Pingguo hydrogeological system, among which 66 are in the southeastern area, and 33 are in the northeastern area. δ and δ^2 were used to measure the circumference and area, and the relationship between lnL(δ) and lnA(δ^2) is shown in Figure 11a. The gradients of the line of lnL(δ) and lnA(δ^2) are the fractal dimensions. The total fractal dimension, the southeastern fractal dimension, and the northwestern fractal dimension are 1.3818, 1.4122, and 1.3561, respectively, and the determination coefficients are 0.8499, 0.8847, and 0.8016, respectively.

There are 63 Karst depressions in the Dongfeng hydrogeological system, among which 36 are in the groundwater deeply buried area, and 27 are in the groundwater shallowly buried area. δ and δ^2 were used to measure the circumference and area, and the relationship between lnL(δ) and lnA(δ^2) is shown in Figure 11b. The total fractal dimension, the fractal dimension in the deeply buried area, and the fractal dimension in the shallowly buried area are 1.4628, 1.43412, and 1.5159, respectively, and the determination coefficients are 0.903, 0.9185, and 0.902, respectively.

The relationships between ln(δ) and ln(N(δ)) in these three typical study areas are shown in Figure 12. The values of δ are 50 m, 100 m, 300 m, 500 m, 1000 m, 3000 m, 5000 m, and 7000 m. Additionally, N(δ) comes from all elevation lines in the study area. According to the fractal dimension in subsystems, the gradients of the straight line are 1.501 and 1.394 in the south area and north area, respectively, in the Pingguo System. In the Dongfeng System, the gradients are 1.126 and 1.123 in shallowly and deeply buried areas, respectively. In the Batang system, the gradients are 1.063, 1.083, and 1.101 in different strata.

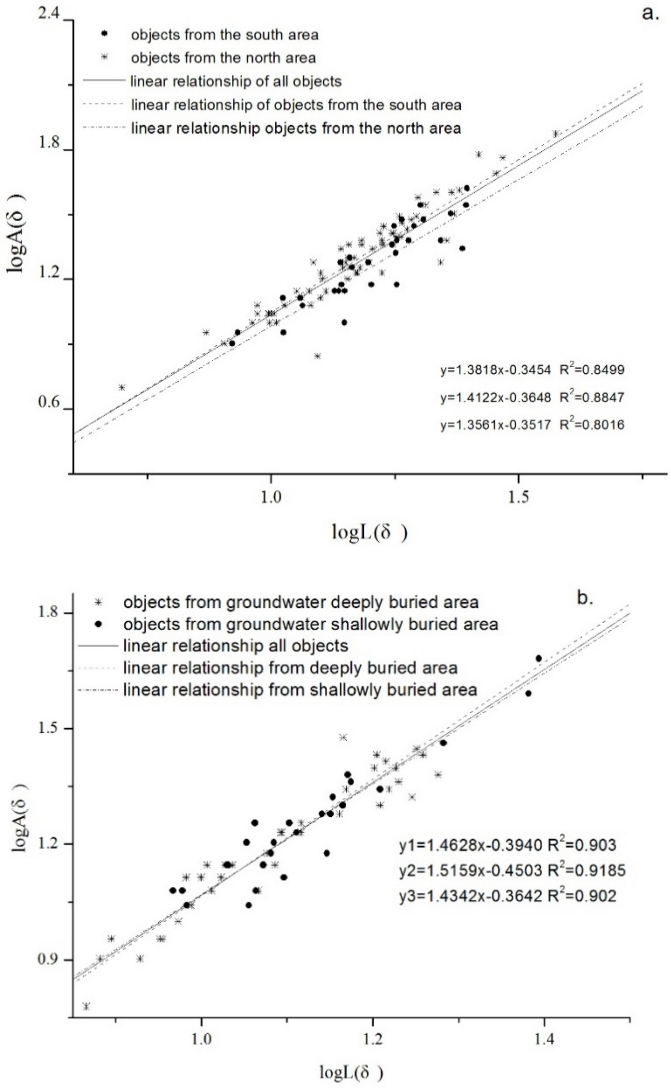

Figure 11. Fractal relationship between area and circumference of polygon connecting the Karst peaks and saddle zones around Karst depressions (shown in Figure 5(a-2,b-2)). (**a**) Pingguo System; (**b**) Dongfeng System.

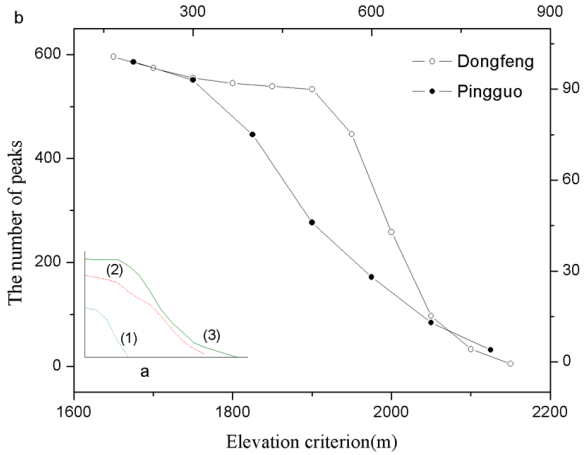

Figure 12. (**a**) Relationship between the height standards and Karst development stages (From Figure 2b). (**b**) Karst development phrase of the Pingguo System and Dongfeng System.

5. Discussions

5.1. Karst Development Characteristics

Typical Karst landforms in the Pingguo System are peak forests, depressions, and isolated hills [4,5]. In the Karst tunnel shown in Figure 5(a-1), there are a few springs with considerable volume, a Karst well, and geological windows. In the area of 141 km^2, there are 99 depression polygons and more than 870 Karst peaks, as shown in Figure 5(a-2). More than two-thirds of them are located in the southeast area where the Karst tunnel passes through. The density of peaks and depressions, and the underground river conduits' appearance, all show strong Karst development. In addition, the results indicated that the topography environment has a more significant influence on the Karst development in this area than the strata [31]. The typical landform in Dongfeng System is shallow plate depressions and hillocks. In the area of 739.5 km^2, there are 63 depressions and more than 597 peaks, as shown in Figure 5(b-2). In this area, the density of peaks and depressions is lower than Pingguo System. There are more springs in this area than in Pingguo System. A larger number of springs with small volumes indicate that the groundwater doesn't intensively excrete. Based on the density of the Karst depressions and peaks and the occurrence of springs in this area, it can be inferred that the Karst development is weaker than that in the Pingguo System. The elevation of the Batang system ranges from 2800 m to 5200 m, the average temperature is about 5 °C, and more than half of the area is higher than the snow line. Currently, there are few Karst depressions in the carbonate area and only a few big valleys distributed in the high elevation area, probably formed by glacier erosion [11,32–34]. There are many springs in this area, and the volume of springs ranges from 0.1 L/s to 500 L/s. All springs emerge from the fracture and faults. The real number of the springs is bigger than shown in Table 1 because most areas are challenging to test. Since no typical Karst landforms emerge, it can be inferred that the Karst development is weak in this area, maybe because it is a Karst in a phase of greater youth.

The fractal characteristics can be used to study the Karst development [25,35–37], and the relationship between the number of peaks and the elevation is used to evaluate the Karst development stage [25,35]. As shown in Figure 12, the relationship in the Pingguo area is similar to the type (2) curve in Figure 2b, which has a slow decreasing trend. However, the relationship in the Dongfeng area is similar to the type (3) curve, with a gentle incline first, then a steep incline, and finally a gentle incline. As shown in Figure 2a,b, curve (3) shows that there are a large number of Karst peaks, and the mountain and the foundation are integrated. Curve (2) shows that the peak bodies are independent, and the basement is integrated. The result shows that Pingguo system is more evolved than Dongfeng system, and the Karst development of the Pingguo System is stronger than that of the Dongfeng System.

The gradient of the relationship line between $\ln L(\delta)$ and $\log A(\delta)$ represents the fractal dimension of Karst depressions [25,35]. The fractal dimension of the Pingguo System is lower than that of the Dongfeng System, as shown in Figure 11. The smaller the fractal dimension, the stronger the Karst development. The fractal dimension in the southeast area is lower than that in the northwest area, which corresponds to the groundwater activity that most springs with big volumes appear in the northwest area (Figure 5(a-1)). In the Dongfeng System, the fractal dimension in the area with shallowly buried groundwater is lower than that in the area with deeply buried groundwater, probably because the springs emerge in the shallowly buried area where the groundwater flow converges. Since it is not a typical Karst depression, the fractal dimension of the Batang system was not obtained.

Table 1. Chemical and isotopic compositions of water samples in the study area where railways pass.

Sample No.	Sample Type [a–e]	Sampling Site [f]	TDS (mg/L)	pH	T (°C)	Na^+	K^+	Mg^{2+}	Ca^{2+}	Cl^-	SO_4^{2-}	HCO_3^-	Charge Balance (%)	$\delta^{18}O$ (‰)	δ^2H (‰)	Exposed Altitude (m)	Supply Altitude (m)	Volume (L/s)	Hydrochemical Type
						(mg/L)													
1	S1	Pingguo Tunnel	-	-	-	-	-	-	-	-	-	-	-	−7.60	−50.6	112	531	-	–
2	S2		606	6.5	23.1	16.2	1.45	4.86	140	17.02	128.72	298	0.73	−7.60	−50.6	112	531	-	$HCO_3 \cdot SO_4$-Ca
3	Grw3		362	7.1	21.2	12.0	1.22	7.78	71.3	11.34	28.82	229	0.94	−7.74	−64.5	118	477	-	HCO_3-Ca
4	Grw4		388	7.2	21.0	12.3	0.85	3.89	81.8	9.98	17.6	262	0.28	−7.81	−49.9	243	437	-	HCO_3-Ca
5	S5		394	7.2	22.3	10.2	1.04	2.43	88.2	11.34	19.21	262	0.71	−7.67	−49.2	154	506	-	HCO_3-Ca
6	Grw6		412	7.1	20.5	5.92	0.39	1.46	97.8	11.8	13.45	281	0.62	−7.32	−53.6	317	553	-	HCO_3-Ca
7	Gr7		416	7.2	22.3	6.35	0.74	4.86	96.2	9.93	19.21	279	2.35	−7.53	−49.1	154	506	-	HCO_3-Ca.Mg
8	S8	Xiaozai Tunnel	374	6.9	22.0	3.21	0.22	14.59	84.3	15.6	1.92	254	9.04	−9.95	−76.9	1208	1492	-	HCO_3-Ca
9	S9		306	7.1	22.0	3.35	0.31	9.73	72.6	11.3	28.8	179	8.69	−9.68	−72.6	1200	1388	-	HCO_3-Ca
10	S10		356	7.3	20.4	25.3	2.73	4.86	71.4	8.51	1.92	241	9.81	−10.3	−78.7	1265	1630	-	HCO_3-Ca.Na
11	R11		134	7.3	21.3	5.24	0.72	3.95	28.9	8.93	17.3	68.7	7.49	−9.52	−69.6	1264	1327	-	HCO_3-Ca
12	Gr12	Changqinpo Tunnel	463	7.1	20.5	32.1	2.11	7.3	80.2	7.09	44.2	290	1.51	−8.57	−70	1100	1154	637	HCO_3-Ca.Na
13	S13		652	7.0	22.1	55.2	4.39	15.56	97.8	9.93	88.4	381	1.92	−10.6	−68.8	1302	1831	11.3	HCO_3.SO_4-Ca.Na
14	S14		984	6.7	20.7	88.1	7.61	39.4	128	18.4	244.0	459	2.06	−10.2	−67.2	1477	1703	-	HCO_3.SO_4-Ca.Na.Mg
15	W15		699	7.3	22.4	59.2	4.21	39.9	77.8	14.2	196.0	308	1.86	−10.1	−66.9	1476	1648	-	HCO_3.Cl.SO_4-Ca.Mg
16	S16	Xingfu Tunnel	-	-	-	-	-	-	-	-	-	-	-	−10.3	−78.8	1390	1789	-	–
17	S17		-	-	-	-	-	-	-	-	-	-	-	−9.29	−74.2	1512	1453	-	–
18	W18		451	6.3	22.7	25.1	1.32	23.8	77.0	70.9	148	105	1.12	−10.2	−67.1	1512	1746	-	HCO_3.Cl.SO_4-Ca.Na Mg
19	Gr19		108	6.5	24.2	13.2	1.12	7.30	8.02	7.55	36.5	34.2	2.23	—	—	-	-	-	HCO_3.SO_4-Ca.Na
20	R20		77.6	6.7	24.5	11.1	0.91	2.43	8.02	7.09	11.5	36.6	3.03	—	—	-	-	-	HCO_3.SO_4-Ca.Na
21	Gr21		102	6.5	27.3	9.0	0.72	2.43	16.0	7.36	15.37	51.3	1.65	−11.3	−70.5	1871	2112	-	HCO_3.SO_4-Ca.Na
22	S22		442	7.1	25.0	31.3	2.23	1.95	84.2	9.93	44.2	268	1.53	−10.4	−70.2	1643	1806	-	HCO_3-Ca.Na
23	S23		364	7.1	22.3	37.2	3.02	8.27	48.9	8.29	38.4	220	1.96	−10.0	−70.0	1459	1695	-	HCO_3-Ca.Na
24	S24		-	-	-	-	-	-	-	-	-	-	-	−10.4	−73.0	1479	1826	-	–
25	S25		-	-	-	-	-	-	-	-	-	-	-	−9.78	−71.4	1590	1618	-	–

Table 1. *Cont.*

Sample No.	Sample Type [a–e]	Sampling Site [f]	TDS (mg/L)	pH	T (°C)	Na^+	K^+	Mg^{2+}	Ca^{2+}	Cl^-	SO_4^{2-}	HCO_3^-	Charge Balance (%)	$\delta^{18}O$ (‰)	δ^2H (‰)	Exposed Altitude (m)	Supply Altitude (m)	Volume (L/s)	Hydrochemical Type
						(mg/L)													
26	Gr26	Xinshao Tunnel	574	7.1	23.1	4.12	0.29	23.8	105	12.0	1.92	427	0.24	−10.3	−78.7	1252	1780	2400	HCO_3-Ca.Mg
27	S27		517	7.1	22.4	8.10	0.65	16.1	101	17.0	13.5	361	0.52	−9.50	−72.7	1245	1639	1050	HCO_3-Ca
28	S28		521	7.1	20.3	1.21	0.07	26.8	92.2	17.0	15.4	369	0.30	−9.86	−75.5	1245	1705	28.3	HCO_3-Ca.Mg
29	S29		397	7.0	19.7	2.10	0.03	19.5	72.1	14.2	32.7	256	0.33	–	–	-	-	22.0	HCO_3-Ca
30	S30	Dongfeng Tunnel	450	7.1	20.2	21.3	1.72	4.86	88.2	14.9	1.97	317	0.95	−10.5	−81.0	1397	1992	330	HCO_3-Ca.Mg
31	S31		441	7.1	20.9	8.11	0.66	3.40	99.4	14.7	2.02	312	0.36	−10.4	−81.3	1397	1947	240	HCO_3-Ca.Na
32	S32		-	-	-	-	-	-	-	-	-	-	-	−10.5	−81.2	1398	1963	-	–
33	S33		432	7.0	20.4	5.31	0.34	4.86	97.8	14.6	1.89	308	0.27	−10.2	−69.5	1467	1872	32.2	HCO_3-Ca.Na
34	S34		493	7.0	21.3	14.0	1.23	3.40	107	11.34	2.29	354	0.68	−9.48	−67.2	1460	1587	12.8	HCO_3-Ca
35	S35		-	-	-	-	-	-	-	-	-	-	0.00	−10.2	−72.9	1424	1861	-	–
36	S36		394	7.0	20.5	1.11	0.03	5.35	91.4	14.6	5.76	276	0.06	−10.6	−84.4	1415	2020	-	HCO_3-Ca
37	Ws37		392	7.1	42.0	12.0	1.09	3.40	84.2	14.3	3.84	273	0.77	−10.9	−86.4	1412	2116	-	HCO_3-Ca
38	Ws38		480	7.1	47.0	10.3	0.82	8.27	100	15.1	4.04	342	0.36	−10.6	−74.1	1435	2027	1440	HCO_3-Ca
39	S39		523	7.1	22.4	5.21	0.44	9.24	116	21.3	17.3	354	0.36	–	–	-	-	1.60	HCO_3-Ca
40	S40		476	7.1	22.7	6.21	0.70	6.32	106	14.9	1.92	341	0.44	−10.8	−75.5	1609	2079	2560	HCO_3-Ca
41	S41		435	7.0	19.5	4.23	0.23	7.30	96.2	13.4	1.92	312	0.54	−9.44	−70.4	1561	1571	39.6	HCO_3-Ca
42	S42		408	7.2	20.9	13.0	1.13	11.2	76.2	17.0	3.84	286	0.88	−10.8	−78.9	1522	2106	268	HCO_3-Ca
43	S43		371	7.2	21.3	12.1	1.01	2.43	80.2	9.93	9.61	256	0.81	−10.8	−82.7	1590	2108	0.30	HCO_3-Ca
44	S44	Shiling Tunnel	454	7.1	21.0	11.4	0.97	4.38	98.6	8.51	13.5	317	0.66	−10.6	−80.9	1730	2002	1300	HCO_3-Ca
45	S45		455	7.0	22.3	9.23	0.79	4.86	100	15.0	5.76	320	0.37	−10.0	−81.2	1691	1795	100	HCO_3-Ca
46	S46	Laoshishan Tunnel	431	7.1	22.7	2.20	0.12	5.35	100	8.51	26.9	288	0.22	–	–	-		34.19	HCO_3-Ca
47	S47		403	7.2	20.2	11.2	0.95	7.30	84.2	14.2	36.5	249	0.74	−10.8	−79	1708	1742	6.00	HCO_3-Ca
48	S48		547	7.7	20.5	9.14	0.73	12.2	114	11.3	38.4	361	0.52	–	–	-	-	-	HCO_3-Ca
49	S49		352	7.3	19.1	2.01	0.07	15.6	64.1	8.51	7.68	254	0.34	−12.2	−89.2	1852	2280	14.6	HCO_3-Ca
50	S50		239	7.3	19.0	7.32	0.33	6.32	45.7	7.91	5.76	166	0.98	−11.6	−83.1	1788	2042	278	HCO_3-Ca
51	S51		513	7.3	19.0	11.3	0.92	9.24	110	5.67	78.8	298	0.60	–	–	-	-	-	HCO_3-Ca
52	S52	Batang tunnel	341	7.8	11.0	6.62	2.31	12.2	53.4	1.15	21.0	244	−5.15	−17.7	−130	2679	4892	-	HCO_3-Ca.Mg
53	S53		334	7.4	10.0	0.53	0.88	24.6	40.7	0.91	15.4	251	−3.82	−17.0	−128	2786	4312	-	HCO_3-Ca.Mg
54	S54		313	7.7	11.3	3.53	0.87	19.0	48.9	0.90	32.9	207	1.08	−17.4	−131	2903	4492	-	HCO_3-Ca.Mg
55	S55		461	7.1	11.1	18.2	1.16	8.49	76.8	1.43	29.6	325	−5.49	−17.6	−130	3936	4558	-	HCO_3-Ca.Mg
56	S56		201	8.0	12.5	0.04	0.11	11.0	31.1	0.68	7.59	151	−3.52	−17.1	−131	3363	4369	-	HCO_3-Ca.Mg
57	S57		227	8.0	12.2	0.11	0.20	12.5	28.5	0.84	7.19	178	−10.88	−18.1	−135	2984	4726	-	HCO_3-Ca.Mg

Table 1. *Cont.*

Sample No.	Sample Type [a–e]	Sampling Site [f]	TDS (mg/L)	pH	T (°C)	Na^+	K^+	Mg^{2+}	Ca^{2+}	Cl^-	SO_4^{2-}	HCO_3^-	Charge Balance (%)	$\delta^{18}O$ (‰)	δ^2H (‰)	Exposed Altitude (m)	Supply Altitude (m)	Volume (L/s)	Hydrochemical Type
						(mg/L)													
58	R58	Batang tunnel	110	8.0	13.0	2.12	0.12	4.01	23.6	0.51	9.19	70.9	8.12	−18.0	−133	3064	4704	-	HCO_3-Ca.Mg
59	S59		338	7.5	15.0	2.85	0.72	3.81	77.6	1.05	38.3	214	0.02	—	—	-	-	-	HCO_3-Ca.Mg
60	S60		288	7.5	12.0	1.06	0.59	9.52	57.8	1.04	30.5	187	0.20	—	—	-	-	-	$HCO_3.SO_4$-Ca
61	S61		283	7.5	14.3	2.17	0.66	7.11	59.5	1.03	32.3	180	0.35	—	—	-	-	-	$HCO_3.SO_4$-Ca
62	S62		183	7.5	12.9	2.12	0.19	2.79	41.2	1.00	8.91	127	1.89	—	—	-	-	-	HCO_3-Ca.Mg
63	S63		263	7.5	14.5	0.01	0.56	7.87	56.1	0.99	35.5	162	0.73	—	—	-	-	-	$HCO_3.SO_4$-Ca
64	S64		375	7.5	13.2	6.20	1.12	12.0	79.8	3.54	83.3	189	3.44	—	—	-	-	-	$HCO_3.SO_4$-Ca

Notes: [a]. S is the sample from springs; [b]. Grw is the groundwater sample obtained through the geological window; [c]. Gr is the groundwater sample from ground river; [d]. R is the water sample from surface river; [e]. Ws is the spring sample from warm spring; [f]. Water samples are classified based on nearby railway tunnels.

Considering all the elevation lines with an elevation difference of 50 m shown in Figure 10, the relationship between lnδ and lnN(δ) was determined, as shown in Figure 13. The gradient of trend lines is considered as the fractal dimensions of elevation lines. The gradients of different systems are in the order of Pingguo System > Dongfeng System > Batang system. For the Pingguo System and Dongfeng System, the Karst landform is Karst depressions, peak-cluster, Karst holes, and groundwater rivers, and the contours are influenced by Karst actions. The bigger the gradient of trend lines, the more complex the contours, and the stronger the Karst development. Therefore, the Karst development in the Pingguo System is stronger than that in the Dongfeng System. In the Batang system, the obvious Karst landforms are Karst depressions, while Karst holes do not appear. Thus, the Karst action has a weak impact on topography, and the gradient of the trend line is the smallest. The strong glaciation and wind erosion in the high elevation area will cause complex contours, but their effects on the contours are weaker than the Karst action.

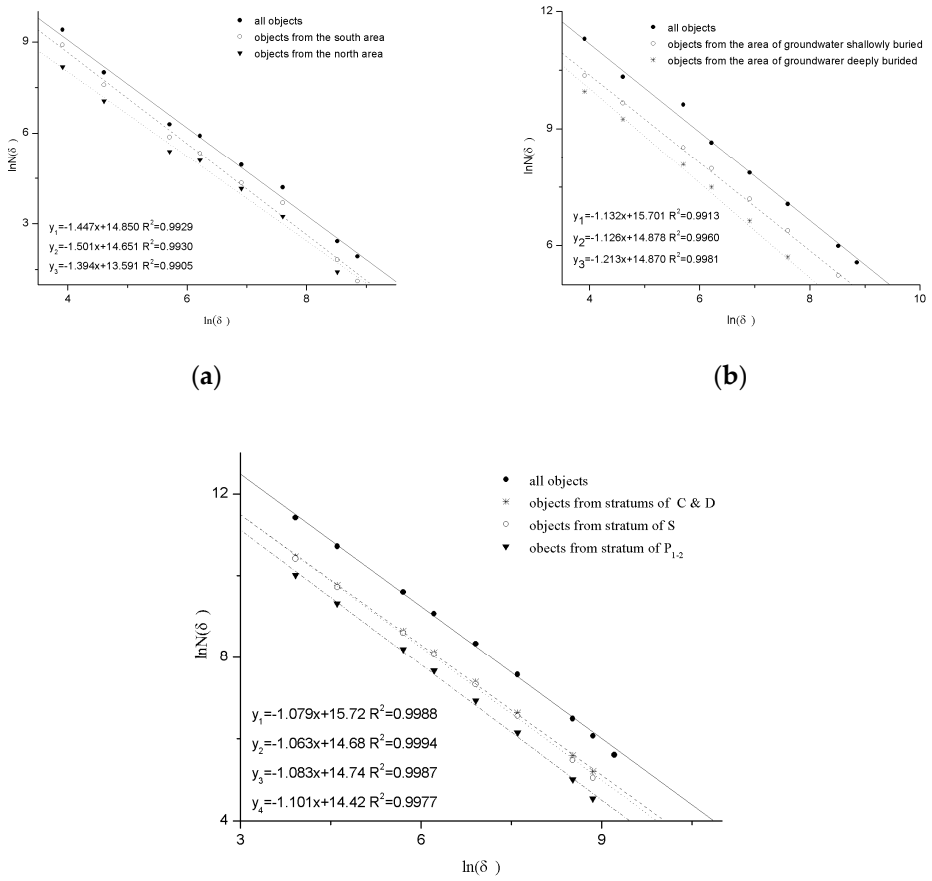

Figure 13. Relationship between lnδ and ln(N(δ)). (**a**) Dongfeng System; (**b**) Batang system; (**c**) Pingguo System.

5.2. Difference in the Groundwater Environment in Three Topography Stages

The saturation index of calcium carbonate and concentration of Ca^{2+} can be used to analyze the seeping conditions [38–40]. The SI-$CaCO_3$ of all groundwater samples (Table 1) are higher than that of surface water samples (in Figure 7), suggesting the water–rock reaction during the groundwater flow. In a closed environment, CO_2 in groundwater cannot be replenished in time, and saturation is often not reached in this condition. The SI-$CaCO_3$ of springs shows a reducing trend from southeast to northwest, as shown in Figure 5(a-1) and Figure 7. In the Pingguo System, a few springs can achieve the calcite saturation phase.

It means that this area has a relatively open condition, which is caused by enough CO_2 supply through many Karst depressions, geological windows, and Karst wells. Along the Yun-Gui railway from east to west, the springs appear from the first stage of topography to the second stage. Near the first stage, a small number of springs in the Pingguo System reach calcite saturation, but in the area further from the first stage, most springs cannot reach saturation, as shown in Figure 7. This phenomenon might be caused by the lower air temperature and less rainfall in the second topography stage area [31,41]. Adapting to this environment, Karst landform becomes shallow plate depressions and hillocks [42,43], the Karst development is weaker, and groundwater is often buried relatively deep in the supply area, as shown in Figure 5(b-1). It means that the environment for groundwater flow is relatively closed, and the supply of CO_2 is insufficient. When springs appear in the slope area from the second to the third topography stage, all springs do not reach saturation shown in Figure 7, and the SI-$CaCO_3$ of No.62 is reduced to −0.9495. In this area, typical Karst landforms, such as Karst depressions and big Karst holes, are not found. Many springs with considerable capacity appear from the slope area instead of the bottom of the valley. In this area, groundwater flows are controlled by large faults and dense cracks. Especially, along the large faults, the groundwater can flow for a long way in a relatively closed environment.

The distribution of δD versus $\delta\ ^{18}$O is influenced by the topographical uplift. The δD and $\delta\ ^{18}$O decrease from southeast to northwest, and concentrate into three zones, as shown in Figure 8, which correspond to the three topography stages. All samples are located near the trend line, which is similar to the southwestern China meteoric line, and the R^2 can reach 0.96. This suggests that there is no "^{18}O shift" in these samples, and the elevation effect of δD versus $\delta\ ^{18}$O can be used to infer the supply elevation of groundwater wells [30]. The elevation difference indicates the hydrodynamics of groundwater. Additionally, the major ions and water molecule isotopes could be used to investigate the hydrodynamic function of Karst aquifer system [44,45]. Overall, the trend of ΔH is in the following order: the third stage > the second stage > the first stage, which shows that the higher topography area may provide stronger hydrodynamics and extend the groundwater flow path. The value of ΔH increases weakly from the first stage to the second stage and is concentrated in these two regions with respect to the third stage area. The ΔH values in the third stage range from ~500 m to 2500 m. This is caused by the length and the width of fractures and faults, and the large faults control the big volume springs with long flow paths.

5.3. Influence of Tunnels on the Groundwater Environment

Tunnels' influence on the groundwater environment is related to not only the Karst development and the characteristics of groundwater flow, but also the tunnel layout [12,18,46]. In addition, the impacts of tunnel excavation on the groundwater include the distribution pattern of water resources, the groundwater flow field, water circulation, groundwater hydrogeochemistry, and water environment [22,47,48]. All these effects occur when the elevation of the tunnel is lower than the groundwater level.

In the first stage topography area, such as Pingguo System, according to the analysis from Sections 5.1 and 5.2, it can be inferred that the Karst is strongly developed and groundwater flows rapidly in this area. It means that the tunnel construction crossing through this area can influence the environment easily and strongly, but different tunnel layouts lead to different influences on the groundwater environment. In Figure 5(a-1), there are two types of tunnel layouts with similar tunnel elevations. The northern layout passes through the hydrogeologic unit I, while the southern layout passes through the hydrogeologic unit II. The presence of springs, the Karst landforms, and the SI-$CaCO_3$ all imply that there is a quicker flow, a more groundwater-bearing stratum, and a lower groundwater level. Whether the north or south layout is used, some portion of the tunnel will be below the groundwater level. During the tunnel construction period, tunnel drainage destroys the aquifer structure, and the groundwater will excrete into the tunnel. As a result, the groundwater level will drop and the springs and the groundwater of geological wells maybe

disappear, or the volume of springs may decrease in the hydrogeological unit. All these influences are weaker in the hydrogeological unit II. In the second-stage topographical area, Karst development, groundwater flow condition, and groundwater-bearing are weaker. All these conditions might cause the vadose zone thinner than the first grade, so tunnels are usually below the groundwater level, and their construction will lower the groundwater level more strongly. If the tunnel does not pass through the discharge area as shown in Figure 5, the spring volume will decrease to some extent but will not dry up. If the tunnel passes through an area covered with the Quaternary aquifer, the Karst collapse will be caused by a drop in the ground level.

In the first grade, the relief of the terrains is relatively small, and the Karst groundwater level is deep and gentle. When the tunnel passes through in the form of shallow burial, the length of the section below groundwater level is limited, and the influence on the Karst water environment is weak, which may lead to the reduction of the flow of some spring points. In the deep-buried tunnel form, the tunnel may be located below the groundwater level for a long distance and reveal the main Karst pipeline, causing the reduction of the groundwater level in a large area and even dry off the springs or underground rivers. The north line of Pingguo Tunnel is parallel to the main runoff direction of s5, s7 springs. Since part of the tunnel is lower than the groundwater level, the flow rate of the springs may be sharply reduced. While the south plan does not cross the runoff area of spring s5, s7, it mainly affects the discharge of the spring s2 by passing through the runoff area of s2. Due to the high Karst development in this area, the groundwater level fluctuates gently. The influence of tunnel drainage on groundwater environment can be effectively reduced or even eliminated by raising the tunnel elevation or avoiding the main runoff channel of groundwater.

In the second grade, the topography fluctuates significantly, and the depth of the groundwater level fluctuates somewhat with the topography. Dongfeng Tunnel is completely below the groundwater level when it passes through, and its distribution direction is basically consistent with the direction of groundwater migration, which will have an impact on spring points within unit II and unit III. If the tunnel direction cannot be changed, the change in tunnel elevation could only change the influence degree of groundwater environment.

In the third grade, the topographic relief is huge and the buried depth of the groundwater level is relatively shallow, but changes with the topographic relief significantly, tunnel construction might be facing a huge head pressure. When the tunnel passes through the slope area from the second to the third stage, as shown in Figure 5c, the typical Karst landforms are not present in the Batang system. The groundwater is bearing in rocks' fractures, and the springs with giant volumes are generally controlled by the large fracture and can flow a long distance. The intense topographical uplift in this area is caused by the collide between the Indian Ocean plate and Eurasian plate, which caused a large number of north–south fractures [49]. If the railway line goes from the second to the third terrain phase, there is no way to avoid this type of fracture. In this area, the groundwater level is high due to the presence of fracture-bearing strata, and tunnels are often located below the groundwater level. The tunnel construction can cause the groundwater level to decrease. Especially, in the area the big fracture passes through, the influence can extend several kilometers [50]. In contrast, in other areas without big faults, the groundwater level and the spring volume only have a weak decrease. Figure 5c shows different layouts with similar elevations in the Batang system, one near the boundary of the river and one in the watershed area. Both cannot avoid meeting with big faults. However, the south layout with a big depth is located in the groundwater recharge area, where the finite depth of fracture development makes weak seeping in deep depth and the influence of the tunnel on the groundwater environment is weak. Relatively speaking, the north layout with a small depth is located in the outlet area of groundwater, where the big fault area has been a strong bearing area for groundwater, and the range of groundwater level is reduced, especially for the fault extending orientation.

Figure 14 shows the relationship between the tunnels' elevation and groundwater level in three topography grades, and it can be inferred that: in the first grade, groundwater

level is low and gentle, while the topographic elevation difference is within 500 m, the water level difference might be less than 100 m, makes it effective to control the tunnel groundwater environment influence by changing the elevation of tunnel. In the second grade, groundwater level changes with the relief variation of the terrain, while the topographic elevation difference ranging from 1000 to 2000 m, and the water level difference could reach hundreds meters, making it hard to control the influence only by changing the tunnel elevation. In the third grade, the huge topographic relief with more than 2000 m of altitude difference also brings a huge water level gap with more than 1000 m. Under such conditions, the variation of tunnel elevation can only extremely limited reduce the impact on groundwater environment

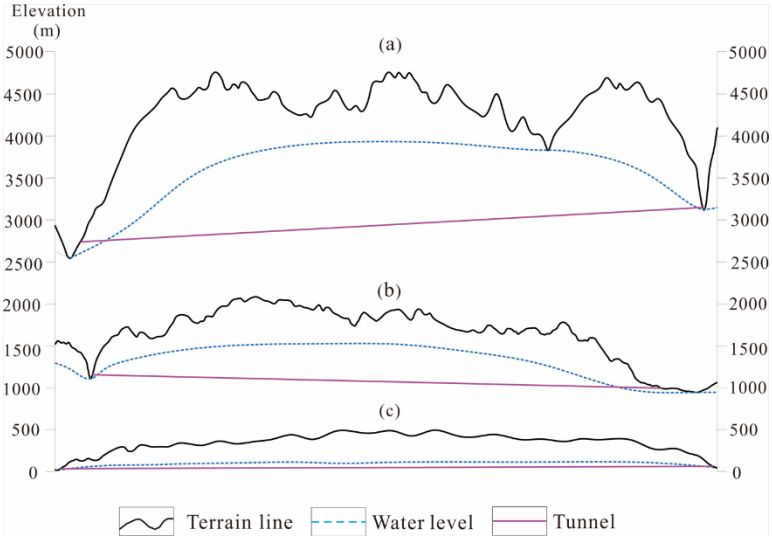

Figure 14. Relationship between tunnel, terrain and groundwater level in three grades. (**a**) Third grade; (**b**) second grade; (**c**) first grade.

6. Conclusions

From the chemical, isotopic, and topography data discussed in this article, Karst development, Karst landforms, and groundwater activities are obviously different in the three topography grade areas of China. The influence of Karst tunnel excavation on the groundwater environment is similar to some extent, and some small differences are present as the terrain rises from the southeast to the northwest area, as shown in Figure 15. In addition, the tunnel layout is a notable factor that may cause detailed differences in impacts.

With the topographical decrease from the second to the first topography area, the Karst development becomes stronger and more complex to some extent. The Karst density and morphology, groundwater confluence, and excretion also suggest that the water-bearing of strata and the flow seeping are stronger in the lower topography. However, if the tunnel elevation is lower than the groundwater level, the influence of groundwater on the environment, including the distribution pattern of water resources, the groundwater flow field, and water circulation, is similar, as shown in Figure 14a,b. In detail, if the tunnel passes through the area near the excretion area of groundwater, depending on the development of Karst, there is a possibility that springs will dry up in the lower topography, and the impact of a drop in the groundwater level might be more significant in this area. Rising the tunnel elevation and avoiding some special sub-hydrogeology systems can effectively reduce the influence. In addition, the relatively weaker Karst development and flow seeping make the vadose zone thinner, and there is less room to raise the tunnel elevation in the second topography area.

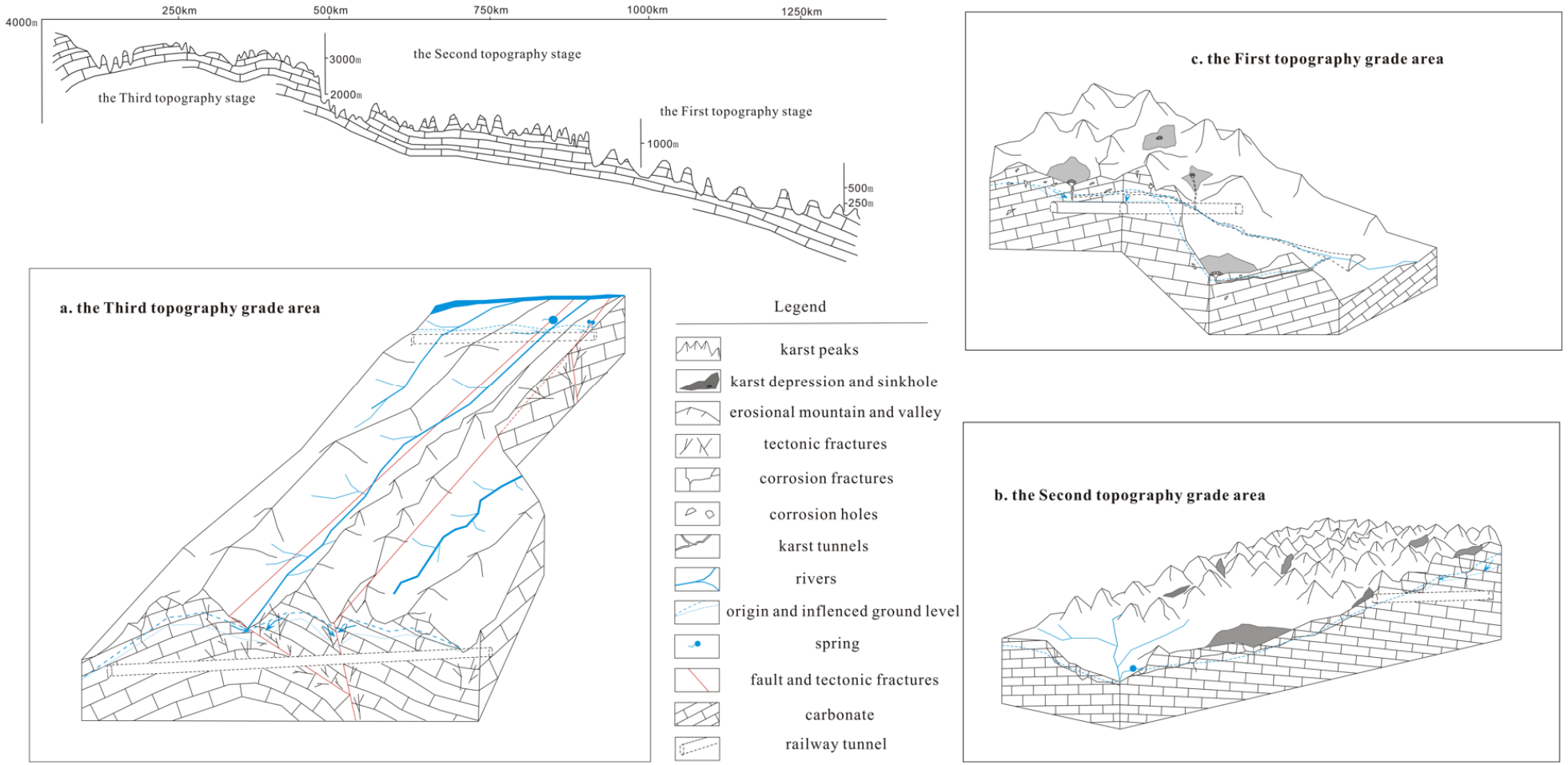

Figure 15. Influence pattern of tunnel excavation on groundwater environment of three topography stages in China.

The topography of the slope area is obviously different from the second grade to the third grade, and there are also obvious differences in the area of the third grade. Typical Karst landforms do not appear in most carbonate rocks area. The groundwater bearing and flow are controlled by the concentrated fracture and giant faults. Based on the huge altitude difference in this area, most tunnels must be below the groundwater level. The strong topography uplift in this area is caused by the collide between the Indian Ocean plate and the Eurasian plate, which leads to a large number of north–south orientation fractures that are not avoidable for transportation routes from east to west. Tunnel excavation encounters giant faults in this area, causing the range of groundwater level to decrease for several miles along the faults extending direction and also diminishing springs controlled by the giant faults. If the tunnel layout is located near the watershed, the deeply buried environment closes the faults, and water hardly seeps into the tunnel, effectively reducing the influence.

Author Contributions: Conceptualization, Q.Z.; Methodology, Q.Z.; Formal analysis, X.L.; Investigation, C.Q. and L.Y.; Writing–original draft, Y.T.; Writing–review & editing, J.Q.; Project administration, M.X. and D.W. All authors have read and agreed to the published version of the manuscript.

Funding: This work was partially supported by the Natural Science Foundation of China's NSFC Grant (No. 41402223).

Data Availability Statement: All data, models, and code generated or used during the study appear in the submitted article.

Acknowledgments: The authors are grateful to the Sichuan Institute of Geological Engineering Investigation Group Co., Ltd.

Conflicts of Interest: The authors declare no conflict of interest.

References

1. Wang, S.J.; Zhang, X.B.; Bai, X.Y. An outline of karst geomorphology Zoning in the karst areas of southern China. *Mt. Res.* **2015**, *33*, 641–648. (In Chinese with English abstract).
2. Wang, P.X. Deformation of Asia and global cooling: Searching links between climate and tectonics. *Quat. Sci.* **1998**, *3*, 213–221, (In Chinese with English abstract).
3. Ying, Y.W.; Tian, W.S.; Ju, J.H. Spatial-Temporal characteristics of temperatures on different terrains of southwest China. *Adv. Clim. Change Res.* **2010**, *6*, 429–435. (In Chinese with English abstract).
4. Zeng, Z.X.; Cheng, M.H.; Yao, Q.Y. The karst morphological characters in south China. *Carsologica Sinica* **1982**, *1*, 27–32. (In Chinese with English abstract).
5. Ren, M.E. *Geomorphic Inheritance and the Development of Tower Karst*; The Commercial Press: Beijing, China, 1987; p. 82.
6. Zhang, D. A morp342.hological analysis of Tibetan limestone pinnacles: Are they remnants of tropical karst tower and cones? *Geomorphology* **1996**, *15*, 79–91.
7. Li, D.W.; Cui, Z.J.; Liu, G.N. Existence of Palaeokarst on Tibet plateau and its correlation with the karst of the eastern district. *Carsologica Sin.* **1999**, *18*, 309–318. (In Chinese with English abstract).
8. Cui, Z.J.; Li, D.W.; Feng, J.L.; Liu, G.N.; Li, H.J. The covered karst, weathering crust and karst(double-level) planation surface. *Sci. China* **2002**, *45*, 365–379. [CrossRef]
9. Hao, Y.; Cao, B.; Zhang, P.; Wang, Q.; Li, Z.; Yeh, T.-C.J. Differences in karst processes between northern and southern China. *Carbonates Evaporites* **2012**, *27*, 331–342. [CrossRef]
10. Wang, F.B. Some problems of karst on Qinghai-Xizang Plateau. *Mt. Res.* **1991**, *9*, 65–72. (In Chinese with English abstract).
11. Zhu, X.W. The nature of Tibet plateau karst and the query concerning "relict fenglin karst". *Carsologica Sin.* **1994**, *13*, 220–227.
12. Lv, Y.X.; Jiang, Y.J.; Hu, W.; Cao, M.; Mao, Y. A review of the effect of tunnel excavation on the hydrology, ecology, and environment in karst areas: Current status, challenge, and perspectives. *J. Hydrol.* **2020**, *586*, 124891. [CrossRef]
13. Vincenzi, V.; Gargini, A.; Goldscheider, N. Using tracer tests and hydrological observations to evaluate effects of tunnel drainage on groundwater and surface waters in the Northern Apennines (Italy). *Appl. Hydrogeol.* **2009**, *17*, 135–150. [CrossRef]
14. Liu, J.; Shen, L.; Wang, Z.; Duan, S.; Wu, W.; Peng, X.; Wu, C.; Jiang, Y. Response of plants water uptake patterns to tunnels excavation based on stable isotopes in a karst trough valley. *J. Hydrol.* **2019**, *571*, 485–493. [CrossRef]
15. Masset, O.; Loew, S. Quantitative hydraulic analysis of pre-drillings and inflows to the Gotthard Base Tunnel (Sedrum Lot, Switzerland). *Eng. Geol.* **2013**, *164*, 50–66. [CrossRef]
16. San, Z.G.; Zhou, C.H.; Yong, G. *The Karst Hydrogeology Condition and Engineering Effects on Yanlongjiang Hydropower Station*; Science Press: Beijing, China, 2018; p. 5.
17. Vázquez-Suñé, E.; Sanchez-Vila, X.; Carrera, J. Introductory review of specific factors influencing urban groundwater, an emerging branch of hydrogeology, with reference to Barcelona, Spain. *Hydrogeol. J.* **2005**, *13*, 522–533. [CrossRef]

18. Kim, Y.-Y.; Lee, K.-K.; Sung, I. Urbanization and the groundwater budget, metropolitan Seoul area, Korea. *Hydrogeol. J.* **2001**, *9*, 401–412. [CrossRef]
19. Gutiérrez, F.; Parise, M.; De Waele, J.; Jourde, H. A review on natural and human-induced geohazards and impacts in karst. *Earth-Science Rev.* **2014**, *138*, 61–88. [CrossRef]
20. Shin, J. Numerical modeling of coupled structural and hydraulic interactions in tunnel linings. *Struct. Eng. Mech.* **2008**, *29*, 1–16. [CrossRef]
21. Deveughèle, M.; Zokimila, P. Impact of an impervious shallow gallery on ground water flow. *Bull. Eng. Geol. Environ.* **2010**, *69*, 143–152. [CrossRef]
22. Li, H.; Kagami, H. Groundwater level and chemistry changes resulting from tunnel construction near Matsumoto City. *Environ. Geol.* **1997**, *32*, 76–84.
23. Vincenzi, V.; Gargini, A.; Goldscheider, N.; Piccinini, L. Differential Hydrogeological Effects of Draining Tunnels Through the Northern Apennines, Italy. *Rock Mech. Rock Eng.* **2014**, *47*, 947–965. [CrossRef]
24. Butscher, C.; Huggenberger, P.; Zechner, E. Impact of tunneling on regional groundwater flow and implications for swelling of clay–sulfate rocks. *Eng. Geol.* **2011**, *117*, 198–206. [CrossRef]
25. Wang, D.; Xu, M. Analysis on Morphologic Features of the Peak-Cluster Depression in Qiubei, Southeast Yunnan. *Log. Sin.* **2010**, *29*, 239–245. (In Chinese with English abstract).
26. Zhu, X.W. New considerations on characteristics and evolution of fenglin karst. *Carsologica Sin.* **1991**, *10*, 171–178. (In Chinese with English abstract).
27. Craig, H. Isotopic Variations in Meteoric Waters. *Science* **1961**, *133*, 1702–1703. [CrossRef] [PubMed]
28. Zhang, H.P.; Liu, E.K.; Wang, D.S.; Jia, Y.K.; Sun, J.C. Composition of stable isotopes of precipitation and controlling factors in China. *Bull Inst. Hydrogeol. Eng. Geol. CAGS* **1991**, *7*, 101–110. (In Chinese with English abstract).
29. Wang, J.; Liu, T.C.; Ying, G. Characteristics of isotope distribution in precipitation in the middle-lower reaches of Yarlung Zangbo River. *Geol. Geochem.* **2000**, *28*, 63–76. (In Chinese with English abstract).
30. Yu, J.; Yu, F.; Liu, D. Hydrogen and oxygen isotopic compositions of meteoric waters in the eastern part of China. *Chin. J. Geochem.* **1987**, *6*, 367–371. [CrossRef]
31. Zuo, J.H.; Luo, Q.; Guo, X.M. Influence on karst development by the three topography grades in China. *Sci. Technol. Inf.* **2012**, *18*, 2010–2013. (In Chinese)
32. Gao, Q.Z.; Cui, Z.J.; Tao, Z.; Liu, G.N.; Hong, Y. The nature, formation age and genetic environment of the Palaeokarst on Qinghai-Xizang Plateau. *Acta Geogr. Sin.* **2002**, *57*, 267–274. (In Chinese with English abstract).
33. Franco, C.; Furio, F. Karst landforms in Friuli Venezia Giulia: From Alpine to coastal karst. *Landsc. Landf. Italy* **2017**, *12*, 147–156.
34. David, J.A.E.; Nigel, A.; Emrys, P. Glacial geomorphology of neutral hills uplands, southeast Alberta, Canada: The pro-cess-form imprints of dynamic ice streams and surging ice lobes. *Geomorphology* **2020**, *35*, 1–40.
35. Gao, W.; Qi, J.H.; Xu, M.; Li, Y.X.; Wang, N.F. Influence of fractal characteristics of a surface karst landform on tunnel construction. *Mod. Tunn. Technol.* **2016**, *53*, 35–43. (In Chinese with English abstract).
36. Li, C.S.; Liao, Y.K.; Ding, J.F. Collapse and water inflow characteristics of a tunnel in metamorphic schist in the nappe structure region. *Mod. Tunn. Technol.* **2017**, *54*, 24–44. (In Chinese with English abstract).
37. Li, C.S.; Liao, Y.K.; Ding, J.F. Feasibility of research on chemical characteristics of karst groundwater by using fractal theory. *J. Eng. Geol.* **2018**, *26*, 464–472. (In Chinese with English abstract).
38. Shen, Z.L. *Hydrogeochemistry*; Geology Press: Beijing, China, 1993; p. 42.
39. Peyraube, N.; Lastennet, R.; Denis, A. Geochemical evolution of groundwater in unsaturated zone of karstic massif, using the Pco2-Sic relationship. *J. Hydrol.* **2012**, *430–431*, 13–24. [CrossRef]
40. Peyraube, N.; Lastennet, R.; Denis, A.; Malaurent, P.; Villanueva, J.D. Interpreting CO_2–SIc relationship to estimate CO_2 baseline in limestone aquifers. *Environ. Earth Sci.* **2014**, *72*, 4207–4215. [CrossRef]
41. Li, D.W.; Cui, Z.J.; Liu, G.N. Feature and origin of covered karst on hunan, Guangxi, Guizhou, Yunnan and Tibet. *J. Mt. Sci.* **2000**, *18*, 289–295. (In Chinese with English abstract).
42. Wang, Y.; Wang, Z.X. Patterns of karst geomorphologica combinations in areas with rich groundwater. *Carsologica Sin.* **2015**, *34*, 314–324. (In Chinese with English abstract).
43. Wang, Y. Vertical zoning of groundwater runoff system in karst plateau. *Carsologica Sin.* **2018**, *37*, 1–8. (In Chinese with English abstract).
44. Hamed, Y.; Ahmadi, R.; Demdoum, A.; Bouri, S.; Gargouri, I.; Hamed, B.D.; Al-Gamal, S.; Laouar, R.; Choura, A. Use of geochemical, isotopic, and age tracer data to develope models of groundwater flow: A case study of Gafsa mining ba-sin-Southern Tunisia. *J. Afr. Earth Sci.* **2014**, *100*, 418–436. [CrossRef]
45. Hamed, Y.; Dassi, L.; Ahmadi, R.; Ben Dhia, H. Geochemical and isotopic study of the multilayer aquifer system in the Moulares-Redayef basin, southern Tunisia/Etude géochimique et isotopique du système aquifère multicouche du bassin de Moulares-Redayef, sud tunisien. *Hydrol. Sci. J.* **2008**, *53*, 1241–1252. [CrossRef]
46. Yuan, D.X. Discussion on karst environment system. *Carsol. Sin.* **1988**, *3*, 179–186. (In Chinese with English abstract).
47. Chae, G.T.; Yun, S.T.; Choi, B.Y.; Jo, Y.; Mayer, B.; Kim, Y.; Lee, J.Y. Hydrochemistry of urban groundwater, Seoul, Korea: The impact of subway tunnels on groundwater quality. *J. Contam. Hydrol.* **2008**, *101*, 42–52. [CrossRef] [PubMed]
48. Butscher, C. Steady-state groundwater inflow into a circular tunnel. *Tunn. Undergr. Sp. Technol.* **2012**, *32*, 158–167. [CrossRef]

49. Wang, C.Y.; Chen, W.P.; Wang, L.P. Temperature beneath Tibet. *Earth Planet. Sci. Lett.* **2014**, *375*, 326–337. [CrossRef]
50. Ford, D.C.; Williams, P.W. *Karst Geomorphology and Hydrology*; Chapman and Hall: New York, NY, USA, 1989.